

Ab-initio calculations of bandgap tuning of $In_{1-x}Ga_xY$(*Y*=N, P) alloys for optoelectronic applications

Muhammad Rashid, Jamil M, Mahmood Q, Shahid M Ramay, Asif Mahmood A, and Ghaithan H M

Citation: Chin. Phys. B, 2021, 30 (**11**): 116301. DOI: 10.1088/1674-1056/abf128
Journal homepage: http://cpb.iphy.ac.cn; http://iopscience.iop.org/cpb

What follows is a list of articles you may be interested in

First-principles study of the co-effect of carbon doping and oxygen vacancies in ZnO photocatalyst

Jia Shi(史佳), Lei Wang(王蕾), and Qiang Gu(顾强)
Chin. Phys. B, 2021, 30 (**2**): 026301. DOI: 10.1088/1674-1056/abc0db

Electronic structure and optical properties of Ge-and F-doped α -Ga_2O_3: First-principles investigations

Ti-Kang Shu(束体康), Rui-Xia Miao(苗瑞霞), San-Dong Guo(郭三栋), Shao-Qing Wang(王少青), Chen-He Zhao(赵晨鹤), and Xue-Lan Zhang(张雪兰)
Chin. Phys. B, 2020, 29 (**12**): 126301. DOI: 10.1088/1674-1056/abbbff

Surface-regulated triangular borophene as Dirac-like materials from density functional calculation investigation

Wenyu Fang(方文玉), Wenbin Kang(康文斌), Jun Zhao(赵军), Pengcheng Zhang(张鹏程)
Chin. Phys. B, 2020, 29 (**9**): 096301. DOI: 10.1088/1674-1056/ab9bff

Electronic structures and optical properties of Si- and Sn-doped β-Ga_2O_3: A GGA+*U* study

Jun-Ning Dang(党俊宁), Shu-wen Zheng(郑树文), Lang Chen(陈浪), Tao Zheng(郑涛)
Chin. Phys. B, 2019, 28 (**1**): 016301. DOI: 10.1088/1674-1056/28/1/016301

Unconventional lattice dynamics in few-layer h-BN and indium iodide crystals

Gan Hu(胡干), Jian-Qi Huang(黄建啟), Ya-Ning Wang(王雅宁), Teng Yang(杨腾), Bao-Juan Dong(董宝娟), Ji-Zhang Wang(王吉章), Bo Zhao(赵波), Sajjad Ali(阿里·萨贾德), Zhi-Dong Zhang(张志东)
Chin. Phys. B, 2018, 27 (**8**): 086301. DOI: 10.1088/1674-1056/27/8/086301

Ab-initio calculations of bandgap tuning of $In_{1-x}Ga_xY$ (Y = N, P) alloys for optoelectronic applications

Muhammad Rashid[1,†], Jamil M[2], Mahmood Q[3,4], Shahid M Ramay[5,‡], Asif Mahmood A[6], and Ghaithan H M[5]

[1] *Department of Physics, Ghazi University City Campus, Dera Ghazi Khan, 32200, Pakistan*
[2] *Department of Physics, COMSATS University Islamabad, Islamabad 44000, Pakistan*
[3] *Basic and Applied Scientific Research Center (BASRC), College of Science of Dammam, Imam Abdulrahman Bin Faisal University, P. O. Box 383, Dammam 31113, Saudi Arabia*
[4] *Department Physics, College of Science, Imam Abdulrahman Bin Faisal University, P. O. Box 1982, Dammam 31441, Saudi Arabia*
[5] *Physics and Astronomy Department, College of Science, King Saud University, Riyadh, Saudi Arabia*
[6] *Chemical Engineering Department, College of Engineering, King Saud University, Riyadh, Saudi Arabia*

(Received 6 February 2021; revised manuscript received 18 March 2021; accepted manuscript online 25 March 2021)

The III–V alloys and doping to tune the bandgap for solar cells and other optoelectronic devices has remained a hot topic of research for the last few decades. In the present article, the bandgap tuning and its influence on optical properties of $In_{1-x}Ga_xN/P$, where (x = 0.0, 0.25, 0.50, 0.75, and 1.0) alloys are comprehensively analyzed by density functional theory based on full-potential linearized augmented plane wave method (FP-LAPW) and modified Becke and Johnson potentials (TB-mBJ). The direct bandgaps turn from 0.7 eV to 3.44 eV, and 1.41 eV to 2.32 eV for $In_{1-x}Ga_xN/P$ alloys, which increases their potentials for optoelectronic devices. The optical properties are discussed such as dielectric constants, refraction, absorption, optical conductivity, and reflection. The light is polarized in the low energy region with minimum reflection. The absorption and optical conduction are maxima in the visible region, and they are shifted into the ultraviolet region by Ga doping. Moreover, static dielectric constant $\varepsilon_1(0)$ is in line with the bandgap from Penn's model.

Keywords: density functional theory, direct bandgap III–V semiconductors, tuning of optical band gap, solar cell applications

PACS: 63.20.D–, 63.20.–e, 71.15.Mb, 72.40.+w **DOI:** 10.1088/1674-1056/abf128

1. Introduction

The shortage of energy supply and increasing its demand have inspired the scientific community to explore the variety of materials for optoelectronic applications since the last two decades. Owing to their bandgap span from infrared region to ultraviolet region, the III–V compounds and their alloys are considered to be potential materials for optical applications.[1–6] For optical systems, the gallium nitride (GaN), gallium phosphide (GaP), and their alloys are of great importance in making low cost, small size, and fast functional blue light-emitting diodes (LEDs), laser diodes, photodetectors, solar cell for visible light, and long-wavelength emitters.[7,8] The knowledge of the bandgap and its engineering during alloy formation is significant for understanding optical properties in a wide range of energy spectrum. The optical behaviors of compounds depend on their desities of states (DOSs) and their investigation is an effective tool for obtaining the true knowledge of electronic structures.[9,10] The III–V binary compounds GaN, InN, GaP, InP, and their alloys ($In_{1-x}Ga_xN$ and $In_{1-x}Ga_xP$) have simple cubic zinc blende (ZB) structures and can be easily grown into the cubic phase.[11]

The nature and range of bandgap play a vital role in selecting the high-efficiency materials for optoelectronic applications. The direct bandgap semiconductors are superior to indirect bandgap semiconductors because phonons induced in the indirect band materials create heating and slow down the absorption of light and recombination rate in optical devices. Ultimately, the device efficiency decreases, thereby ejecting such materials from the market of the electronic industry.[12–18] The GaN (E_g = 3.44 eV), InN (E_g = 0.7 eV), and InP (E_g = 1.35 eV) are direct band semiconductors operating in an ultraviolet to infrared region of spectrum while GaP (E_g = 2.26 eV) is indirect bandgap semiconductor in visible region.[19–22] The alloy formation of $In_{1-x}Ga_xN$ and $In_{1-x}Ga_xP$ tune the bandgap from 0.7 eV to 3.44 eV and 1.35 eV to 2.26 eV to explore the highest efficiency in infrared, visible, and ultraviolet regions. This is the direct and easiest approach to the investigating of the bandgap-dependent electronic behavior and optical response of these semiconductor systems.

From an experimental viewpoint, InGaN and InGaP are evidenced to be the most suitable systems for photovoltaic applications in which In content ranges from 0% and 100%. The InGaN-based solar cells demand the 2.4 eV, and the InGaP-

†Corresponding author. E-mail: rapakistana@yahoo.com, mrashid@gudgk.edu.pk
‡Corresponding author. E-mail: schaudhry@ksu.edu.sa
© 2021 Chinese Physical Society and IOP Publishing Ltd

based solar cells requires 1.5-eV bandgap in the visible region for maximum efficiency which is obtained by changing the In content.[23,24] The multi-junction solar cells for ultra-high efficiency can be achieved by depositing the thin epitaxial layer of $In_xGa_{1-x}N$ on a GaN substrate. This condition is unsettled at a high In concentration due to the lattice mismatch between substrate and thin film, caused by phase separation and structural defects.[25] However, at lower content of In quantum confinement, the hetero-structure of InGaN/GaN possesses the larger quality and stability. Furthermore, it has been elaborated that an In fraction of 30%–40% is the best suitable for the InGaN-based solar cells. This proportion is achieved by minimizing the phase separation and lattice mismatch problems and also by the high performance of solar cells at longer wavelengths.[26] Therefore, quantum well structures of InGaN with a 25-Å-thick layer evidence a drastic improvement in photoluminescence (PL) intensity. On the other hand, the quantum efficiency of green-emitting LED of InGaP system is 10% in hexagonal phase but the phase transformation from cubic to hexagonal phase converts the indirect bandgap into direct bandgap, which has not yet been certified experimentally. The theoretical work of Ample Laref explains the optical behaviors of the $In_{1-x}Ga_xN$ and $In_{1-x}Ga_xP$ through the full-potential linearly augmented plane wave method by changing the indium content but the provided description is limited.[22,27,28] Therefore, it is needed to explore them comprehensively.

In the present work, the electronic and optical behaviors of studied materials are elucidated by the PBE–GGA approximation[29] and electronic bandgap is evaluated by the most versatile Trans Balaha modified potential (TB-mBJ).[30] The optical behavior is analyzed according to the composition variation of Ga ions in the InP and InN and pressure insertion. The techniques, pressure variation, and composition variations tailor the bandgap for the highest absorption of light to increase optical efficiency for solar cell applications. The details of optical properties are discussed in terms of dielectric constants, refraction, dispersion, polarization, absorption, and optical loss factor.

2. Method

To investigate the optical measurements of Ga-doped InN & InP alloys, we perform the simulation by the DFT-dependent full-potential linearized augmented plane wave method through the Wein2k code. The studied compounds are relaxed and optimized to calculate the ground state parameters in the Zinc blend phase in the PBE-sol approximation which is more accurate than local density approximation (LDA).[31,32] To determine the Hamiltonian of the system, optimized structures are converged by self-consistent field. In Hamiltonian, exchange–correlation energy (E_{xc}) is generally approximated by the familiar LDA, GGA, or hybrid approximations.[33,34] These approximations are generally used to find precise parameters for the ground state while excited state properties are undervalued. For instance, the bandgap described through these approximations is robustly undervalued. The difficulty related with the above said approximations lies in undervaluing the bandgap which is self-interaction error and limiting the derivative discontinuity. On the other side, the hybrid functional is more costly and $\mathrm{LDA}+U/\mathrm{GGA}+U$ are restricted to localized states.[35] Therefore, to elucidate the above problems, Trans and Blaha,[36] and Koller *et al.*[37] improved Backe–Johnson potential (TB-mBJ) by precisely computing the electronic structures of semiconductors, insulators, and metal oxides. The optical properties related to the bandgap are calculated by using this potential effect. Furthermore, the solutions of the wave function are divided into two circumstances: one is the spherical harmonic-type solution in the muffin-tin region where the core electrons are kept and the other is the plane wave-like wave function in the remaining region. The convergence of eigenvalues is achieved by taking $K_{\max} = 8.0/R_{\mathrm{MT}}\ (\mathrm{Ryd})^{1/2}$ for cut-off energy. The total energy value converges to 10^{-4} Ryd/unit cell in self-consistent calculations. We take $4000k$ points of the k-mesh grid because energy released from the alloys in charge/energy convergence becomes constant at this or above value.

3. Results and discussion

3.1. Structural and electronic properties

The crystal structures of $In_{1-x}Ga_xN/P$, where ($x = 0.0$, 0.25, 0.50, 0.75, and 1.0) are plotted in Figs. 1(a)–1(e). The InN/P and GaN/P both have a binary structure belonging to the space groups 216_F-43m while doped $In_{0.75}Ga_{0.25}N/P$ and $In_{0.25}Ga_{0.75}N/P$ both have a structure belonging to space group 215_P-43m. The structure of $In_{0.50}Ga_{0.50}N/P$ belongs to space group 115_P-4m2. We can convert this tetragonal space group into cubic group by SQS or SAE whose detailed description can be found in Refs. [38,39].

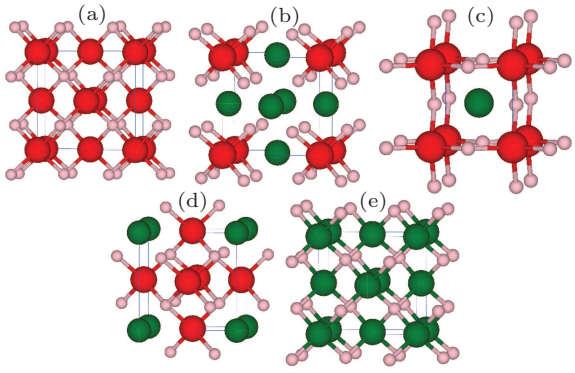


Fig. 1. The crystal structures of panel (a) InN/P, (b) $In_{0.75}Ga_{0.25}N/P$, (c) $In_{0.50}Ga_{0.50}N/P$, (d) $In_{0.25}Ga_{0.75}N/P$, and (e) GaN/P.

In the system under study, the space group is selected and used for the convenience of convergence of energy. The electronic behaviors of $In_{1-x}Ga_xN/P$, where ($x = 0.0$, 0.25, 0.50, 0.75, and 1.0) are illustrated by using lattice constant a_0 (Å), electronic band gap E_g (eV), and total density of states (TDOS). The lattice constant is optimized to relax the structures of Ga doped InN/P alloys. The lattice constant decreases with concentration of Ga atoms increasing because In (2.2 Å) atom has a greater atomic radius than Ga atom (1.87 Å) as shown in Fig. 2(a). The bandgap increases with Ga atom concentration increasing because the smaller size of the Ga atom shrinks the density of states away from the forbidden energy region. The increasing trend of band gap for Ga atoms doped InN/P is shown in Fig. 2(b). The accuracy of the results can be ensured from the binary InN/P and GaN/P band gaps, which is consistent with those reported in Refs. [40–45].

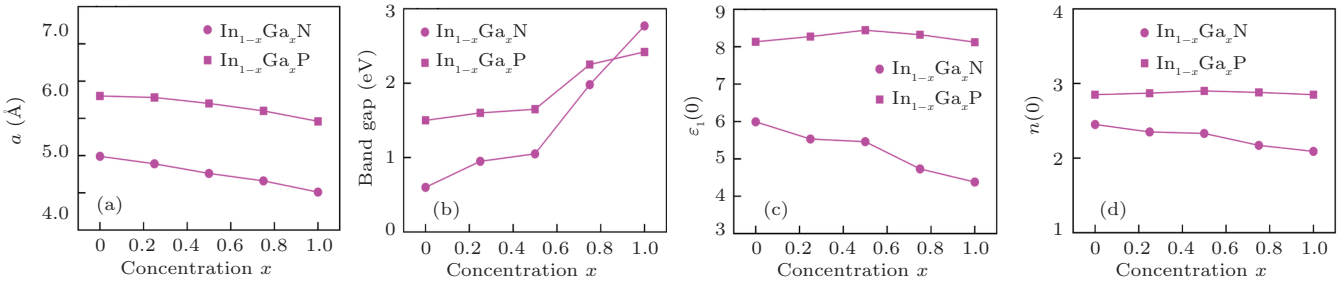


Fig. 2. Calculated lattice constant, band gap, static dielectric constant and refractive index of $In_{1-x}Ga_xN/P$ ($x = 0.0$, 0.25, 0.50, 0.75 and 1.0).

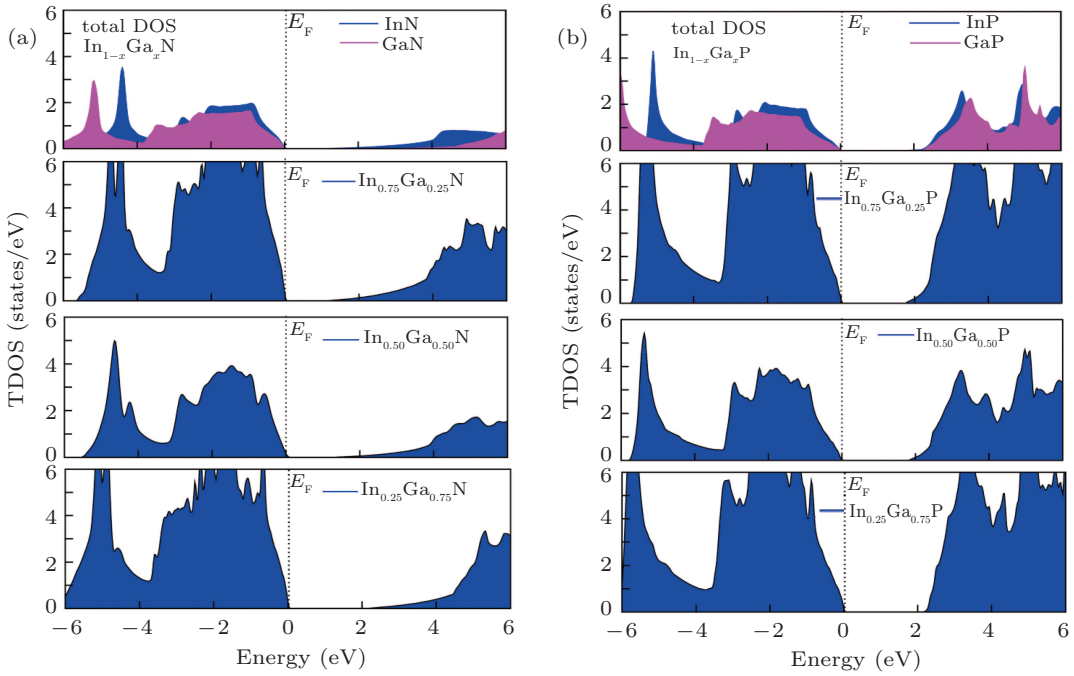


Fig. 3. Total density of states (TDOS) and partial density of states (PDOS) of (a) $In_{1-x}Ga_xN$ and (b) $In_{1-x}Ga_xP$, where $x = 0.0$, 0.25, 0.50, 0.75, and 1.0.

Moreover, to see the detailed electronic picture of binary structure and doped compounds, the total densities of states are plotted in Figs. 3(a) and 3(b). The band gaps of binary structure and doped compounds reported in Fig. 3(b) are similar to those from a density of states in Fig. 3. The InN/P band gap indicates that the maximum absorption region is visible while the doping of Ga leads it to shift to the ultraviolet region. Therefore, with the help of bandgap tuning, the optoelectronic devices can be fabricated with desired energy range, thereby increasing the potential applications of studied materials in solar cells and other optoelectronic devices. To explore the optical behavior of studied materials, their optical parameters will be analyzed in detail below.

3.2. Optical properties

The optical properties of a semiconductor have dynamic significance due to their valuable information on a large scale that can be taken in our efforts to understand the properties of semiconductors, especially for optoelectronic applications in the direct bandgap materials. In optoelectronic $In_{1-x}Ga_xN/P$ motivates the researchers to explore them. The direct transition from the valence band to conduction bands takes place. The maxima of the valence band and minima of the conduction band at the same symmetry points form a direct bandgap that creates easy transition of electrons valence band to con-

duction band with energy loss decreasing. The efficiency of light-emitting device is enhanced due to the recombination rate rising.[46–50] The optical response in the existence of an external electric field of any physical system can be specified in terms of dielectric function $\varepsilon(\omega) = \varepsilon_1(\omega) + \mathrm{i}\varepsilon_2(\omega)$. The Kramer–Kronig relation[42] is used to calculate the real part of dielectric function $\varepsilon_1(\omega)$ that explains the dispersion of light from matter surface. The absorption of electromagnetic radiations is explained by the complex dielectric function of imaginary part $\varepsilon_2(\omega)$. The dielectric constant of frequency-dependent real part and imaginary part are obtained from the Kramer–Kronig relation[22] as follows:

$$\varepsilon_1(\omega) = 1 + \frac{2}{\pi} \mathrm{P} \int_0^{\infty} \frac{\omega' \varepsilon_2(\omega')}{\omega'^2 - \omega^2} \mathrm{d}\omega', \tag{1}$$

$$\varepsilon_2(\omega) = \frac{e^2\hbar}{\pi m^2 \omega^2} \sum_{\mathrm{BZ}}^{\infty} \left| M_{cv}(k) \right|^2 \delta[\omega_{cv}(k) - \omega] \mathrm{d}^3 k, \tag{2}$$

where the principal integral value is represented by P, and k is the wave vector within the first Brillion zone (BZ) boundary. The Kramer–Kronig relation is used to solve the constituents of dielectric tensor between the real and imaginary part that explain photon matter interaction.

The calculated $\varepsilon_1(\omega)$ and $\varepsilon_2(\omega)$ for $In_{1-x}Ga_xN$ are presented in Figs. 4(a) and 4(b), and for $In_{1-x}Ga_xP$ in Figs. 4(c) and 4(d). The real part of dielectric constant $\varepsilon_1(\omega)$ explains the material polarization when it exposes to electromagnetic radiation. The value of $\varepsilon_1(\omega)$ increases from zero energy value and to the values of the first resonance at 1 eV, 1.8 eV, 2.1 eV, and 2.5 eV for $In_{1-x}Ga_xN$ alloys. The peak values of the second resonance occur between 6 eV and 7 eV because of matching the light and materials vibration frequency. The peaks between 6 eV and 12 eV have large variations because of different resonance frequencies. At high energy, plasma resonance breaks and peaks minimize to a negative value between 9 eV to 16 eV with a minimum value at 12 eV. The $In_{1-x}Ga_xN$ alloys show metallic response in this energy region because of bandgap incompatibility with the energy of incoming light. While for $In_{1-x}Ga_xP$ alloys, the $\varepsilon_1(\omega)$ reaches a peak value at 3 eV for InP and then shifts toward higher energy up to 4 eV for GaP by increasing the Ga atom concentration, as shown in Fig. 4(c), then monotonically drops to a minimum value at 5 eV, becoming negative which shows the metallic character. Therefore, all the light is reflected from the material surface. The materials behave as a superluminal-type material because negative values of $\varepsilon_1(\omega)$ make the susceptibility and permeability negative like left-handed-type materials which have not been discovered yet.[51–53] Figures 4(a) and 4(c) show that the static dielectric constant $\varepsilon_1(0)$ is dependent on material bandgap. By increasing the Ga atom concentration in InN/P, the value of static dielectric constant $\varepsilon_1(0)$ increases. The Penn's model $\varepsilon_1(0) \approx 1 + (h\omega_\mathrm{p}/E_\mathrm{g})^2$,[54] (where E_g and $h\omega_\mathrm{p}$ are the bandgaps and plasma frequency of the material) is exactly related to band gaps.

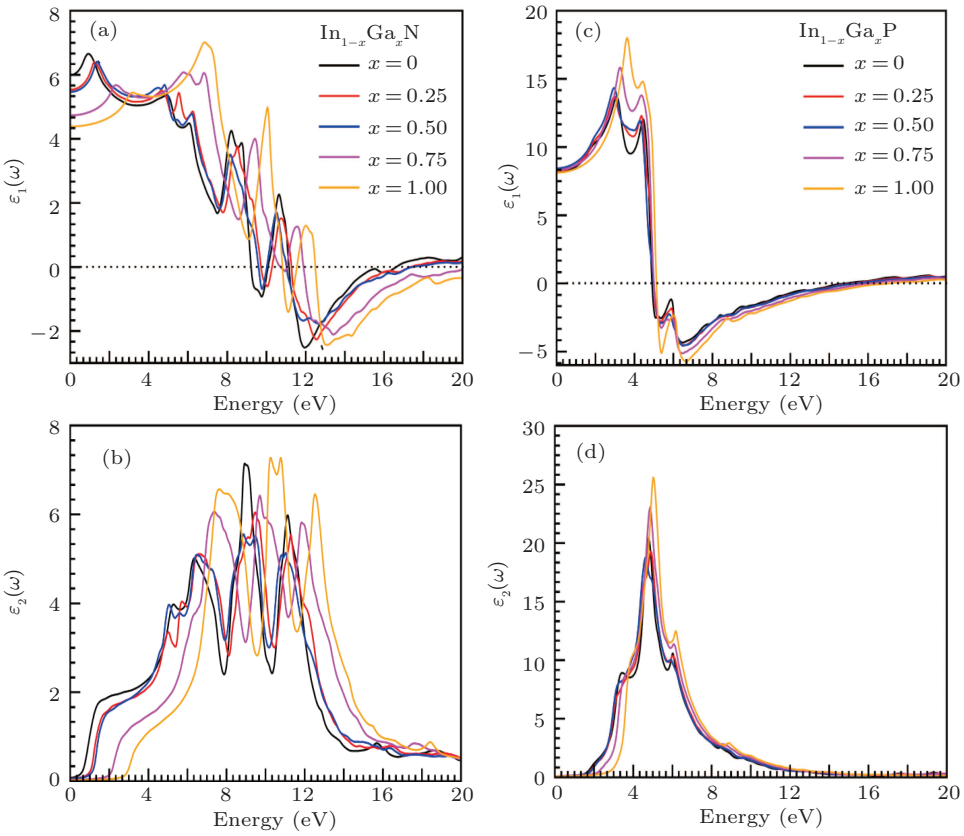


Fig. 4. Real part and imaginary part of dielectric constant of [(a) and (b)] $In_{1-x}Ga_xN$, and [(c) and(d)] $In_{1-x}Ga_xP$ for $x = 0.0$, 0.25, 0.50, 0.75 and 1.0.

For the construction of optoelectronic device, the imaginary part of the dielectric constant $\varepsilon_2(\omega)$ has a significant role. The light energy is measured to attenuate when the electromagnetic wave of suitable frequency passes through a material medium. The calculated values of the absorption coefficient for $In_{1-x}Ga_xN/P$ alloys are plotted in Figs. 4(b) and 4(d). The threshold value of the absorption coefficient is the limit from which material starts the absorption of light. These measured optical band gaps and the band gaps measured from band structures (Fig. 2(b)) are consistent with each other, which shows the reliability of our calculated results. Moreover, the band gaps calculated from binary structures InN/InP and GaN/GaP are matched with the experimental band gaps 0.71 eV/1.42 eV and 3.44 eV/2.32 eV.[40–42] The $\varepsilon_2(\omega)$ increases with Ga doping in InN and attains the first maximum peak at 6 eV, then at 9 eV, and finally at 11 eV. The different peaks of absorption occur because of different light–matter interactions and different energy delivering rates of photons to electrons. The doping of Ga atoms shifts the absorption peaks towards high energy. For $In_{1-x}Ga_xP$ alloys, maximum absorption occurs at 5 eV as shown in Fig. 4(d). The absorption bands for $In_{1-x}Ga_xN$ alloys lie between 1 eV and 14 eV while for $In_{1-x}Ga_xP$ alloys between 2 eV and 8 eV. Therefore, the tuning of band gaps makes the studied alloys suitable for visible and ultraviolet optoelectronic applications.

The other optical parameters like refractive index $n(\omega)$ and extinction coefficient $k(\omega)$ are related to the photon energy–matter interaction and calculated as a function of $\varepsilon_1(\omega)$ and $\varepsilon_2(\omega)$ as follows:

$$n(\omega) = \left[\frac{\varepsilon_1(\omega)}{2} + \frac{\sqrt{\varepsilon_1^2(\omega)+\varepsilon_2^2(\omega)}}{2}\right]^{1/2}, \tag{3}$$

$$k(\omega) = \left[\frac{-\varepsilon_1(\omega)}{2} + \frac{\sqrt{\varepsilon_1^2(\omega)+\varepsilon_2^2(\omega)}}{2}\right]^{1/2}. \tag{4}$$

The complex refraction coefficient is related to the complex dielectric constant and expressed as

$$\bar{n}(\omega) = n(\omega) + \mathrm{i}k(\omega).$$

The refractive index $n(\omega)$ and extinction coefficient $k(\omega)$ are related to the real part and the imaginary part of the dielectric constant through the following equations $n^2 - k^2 = \varepsilon_1(\omega)$ and $2nk(\omega) = \varepsilon_2(\omega)$ as shown in the following Figs. 5(a) and 5(c).

The zero-frequency values of refractive index $n(\omega)$ for $In_{1-x}Ga_xN$ $In_{1-x}Ga_xP$ alloys are presented in Fig. 2(d). It shows that $n(0)$ decreases with the augment of Ga atom concentration and the absorption region shifts from visible to near-ultraviolet region with the transparency changing. Moreover, the static refractive index $n(0)$ and real part of dielectric constant $\varepsilon_1(0)$ exactly follow the relation $n(0) = \varepsilon_1^2(0)$ as shown in Fig. 1(c) and Fig. 2(d).[55–57] The value of refractive index increases from static value and reaches to 8 eV (InN), 1.2 eV (0.25, 0.5), 2 eV (0.75), and 3 eV (GaN). The three fluctuating peaks at 6 eV, 9 eV, and 11 eV are recorded which are related to the real part of the dielectric constant due to the same reason as that explained above. Furthermore, for $In_{1-x}Ga_xP$ alloys, it reaches 3 eV and 4.4 eV and then drops to minimum values. For vacuum, the absorption is zero and the refractive index is one, the increasing value of the refractive index shows that the light is absorbed by the material. Hence, the increasing of refractive index reduces the speed of light. From 12 eV for $In_{1-x}Ga_xN$ and 9 eV for $In_{1-x}Ga_xP$, the value of refractive index becomes less than one, which increases the phase velocity $(v = c/n)$ higher than speed of light. Therefore, the material becomes metallic and lift handed type as explained above for negative value of refractive index.[58–60]

The metallic response allows a longer wavelength $\lambda = \lambda_0/n$ and minimum photon energy $E = hc/\lambda$. Moreover, the doping shifts the negative region to a higher value and transfers the operative absorption from the visible to the ultraviolet region that is justified by the increasing bandgap of studied alloys. The extinction coefficient $k(\omega)$ has a similar behavior to $\varepsilon_2(\omega)$. The calculated values of $k(\omega)$ are presented in Figs. 5(b) and 5(d) for $In_{1-x}Ga_xN$ alloy and $In_{1-x}Ga_xP$ alloy. The values for InN are high at 5 eV, 7 eV, and 11 eV, and with doping Ga they shift to higher energy while for $In_{1-x}Ga_xP$ alloys, the peaks are at 5 eV and then decrease to minimum values with doping of Ga atoms. In the $In_{1-x}Ga_xP$ alloys, a little bit of variations in the values of $\varepsilon_2(\omega)$ and $k(\omega)$ may be due to theoretical approximations.

The absorption coefficient $\alpha(\omega)$ is another parameter that measures whether the materials are suitable for solar and other optoelectronic applications or not. The reported values of the absorption coefficient for $In_{1-x}Ga_xN/P$ alloys are presented in Figs. 6(a) and 6(c). They measure the decay of the photon energy per centimeter into the material. The behavior of the absorption coefficient $\alpha(\omega)$, the imaginary part of the dielectric constant $\varepsilon_2(\omega)$, and the extinction coefficient $k(\omega)$ are consistent, showing that the Kramer–Krong relation and the tensor matrix equally solve the optical parameters. Moreover, the absorption is linked with the extinction coefficient by the following expression:

$$\alpha(\omega) = 4\pi k(\omega)/\lambda. \tag{5}$$

This relation shows that the absorption coefficient is the product of the wave vector and the extinction coefficient.

The optical conductivity $\sigma(\omega)$ implies the flow of carriers when surplus photon energy is delivered to electrons in the valence band. The electrons move to the conduction band by overcoming the influence of nuclei, and thus increasing the optical current or photocurrent.[61] The calculated values of optical conductivity for the studied alloys are presented in Figs. 6(b) and 6(d).

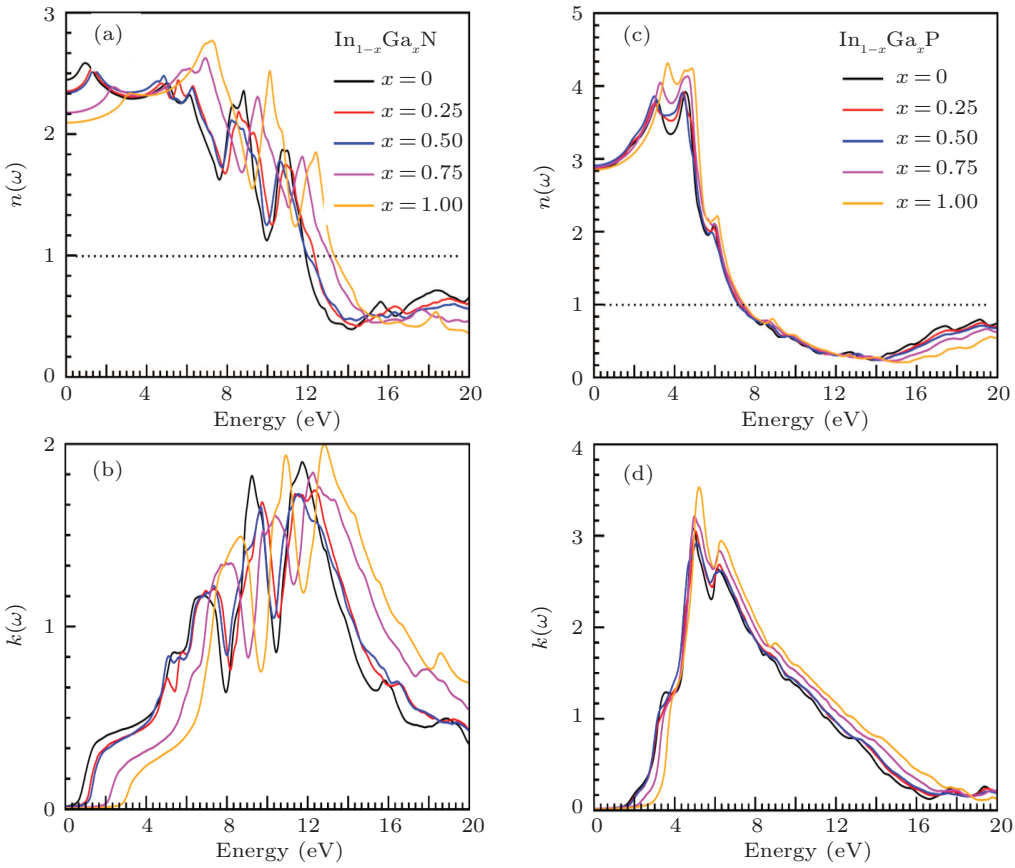


Fig. 5. Refractive index and extinction coefficient of [(a) and (b)] $In_{1-x}Ga_xN$, [(c) and (d)] $In_{1-x}Ga_xP$ with $x = 0$, 0.25, 0.50, 0.75, and 1.0.

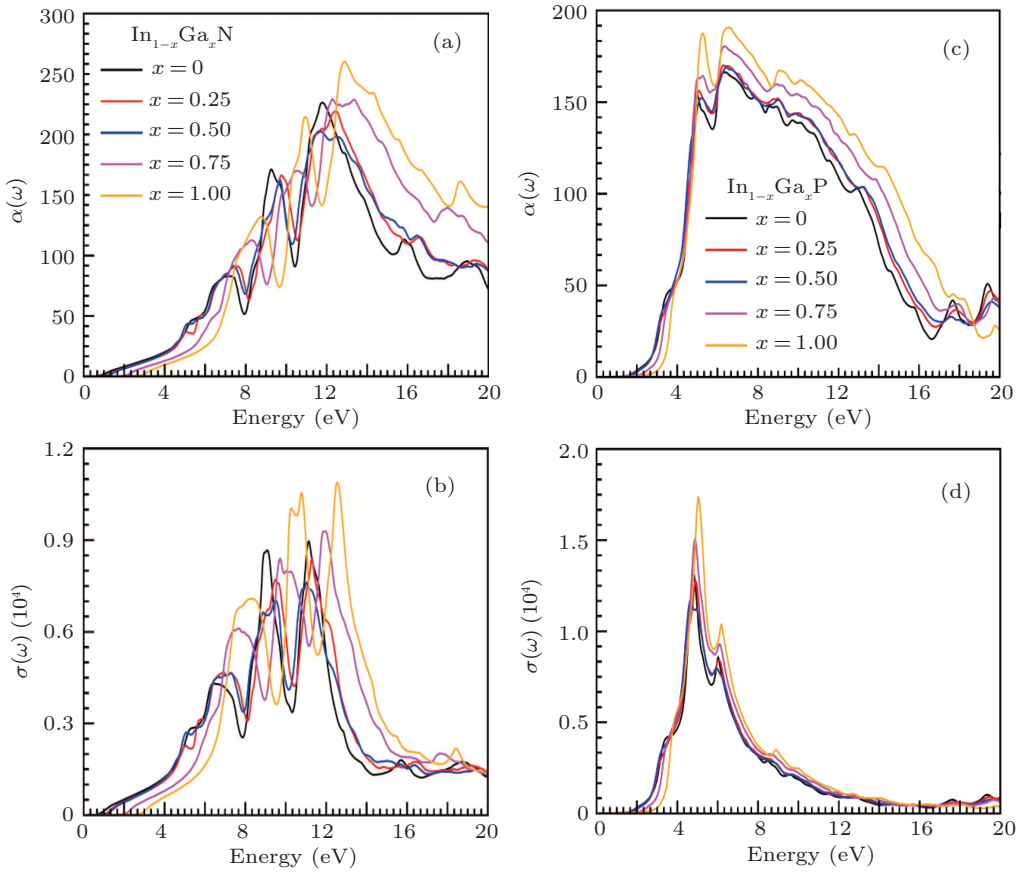


Fig. 6. Absorption coefficient and optical conductivity of [(a) and (b)] $In_{1-x}Ga_xN$ and [(c) and (d)] $In_{1-x}Ga_xP$ with $x = 0.0$, 0.25, 0.50, 0.75, and 1.0, respectively.

During the light–matter interaction, the absorption, transmission, and conduction take place simultaneously. When the energy of the incident photons exceeds the bandgap, the kinetic energy of electrons increases and the electrical conductivity increases accordingly. Moreover, the optical conductivity is related to the dielectric constant by the following expression:

$$\varepsilon(\omega) = \varepsilon_0 + \mathrm{i}\sigma(\omega)/\omega,$$

where ε_0 and ω are the permittivity of the free space and plasma frequency.

Therefore, the optical conductivity is related to the imaginary part of the dielectric constant. It peaks at 9 eV and 11 eV for InN and at 10 eV and 13 eV for GaN, which shows that the optical conductivity peaks shift to higher energy by replacing Ga atom with In atom. On the other hand, the optical conductivity reaches a peak value at 5 eV for $In_{1-x}Ga_xP$ alloys. After attaining peak values, it decreases to a minimum value. The reason has been explained above, and the metallic nature of material in high energy lies in reflecting the light. The largest optical conductivity is found in the visible to the ultraviolet region of the spectrum.

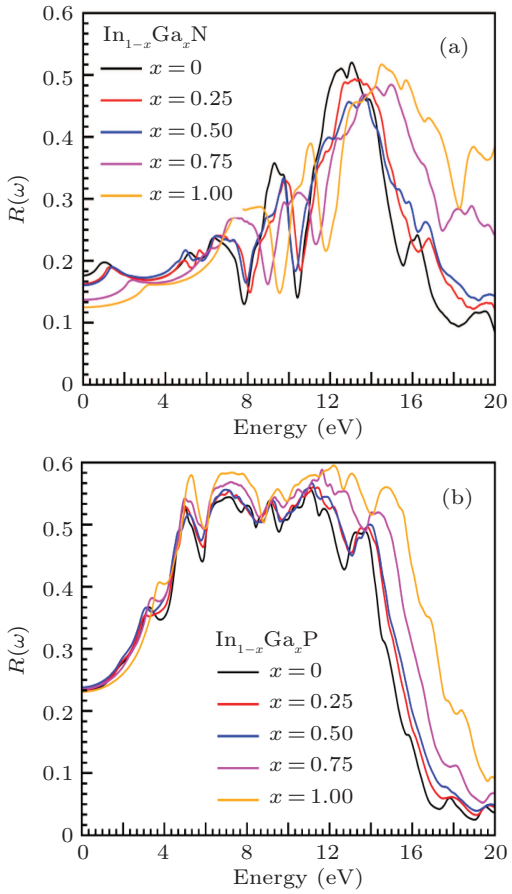


Fig. 7. Reflectivity of (a) $In_{1-x}Ga_xN$, (b) $In_{1-x}Ga_xP$, where $x = 0.0$, 0.25, 0.50, 0.75 and 1.0.

The reflection coefficient $R(\omega)$ is the incident-to-reflected light energy ratio which provides information about surface morphology.[62] It can be calculated from the refractive and extinction coefficient from the following relation:

$$R = \frac{(n-1)^2 + k^2}{(n+1)^2 + k^2}. \tag{6}$$

The reflectivity decreases by doping Ga atoms into InN. A similar trend is found in Ga-doped InP. Its value increases smoothly up to 6 eV for $In_{1-x}Ga_xN$ alloys, and a large fluctuation occurs due to the surface roughness and scattering of light at different angles. However, the maximum reflection zone for $In_{1-x}Ga_xN$ alloys is between 10 eV and 16 eV while for $In_{1-x}Ga_xP$ alloys is between 4 eV and 16 eV as shown in Figs. 7(a) and 7(b). It is also noted that the reflectivity increases with Ga content increasing because of atomic size changing but this effect is minor.

4. Conclusions

In the present study, the electronic and optical properties of $In_{1-x}Ga_xN/P$ ($x = 0.0$, 0.25, 0.50, 0.75, and 1.0) alloys are analyzed by using a full-potential linearized augmented plane wave method and modified Becke and Johnson potential (TB-mBJ). The lattice constant decreases by doping Ga atoms into InN/P because of the smaller atomic size of Ga atom than that of In atom. The bandgap increases from 0.7 eV to 3.44 eV, and 1.41 eV to 2.32 eV with increasing the Ga content. The maximum absorption region shifts from the visible region to the ultraviolet region; therefore, the tuning of the bandgap increases the potential applications of alloys in solar cell and other opto-electronic devices. The static dielectric constant $\varepsilon_1(0)$ and band gap are consistent with those from the Penn's model. The dispersion and polarization of light are maxima in low energy region while the highenergy region behaves as a metal. Reflection of light is less in the energy region where absorption and optical conductivity are stronger, therefore, visible light solar cells possess the favored applications in the low doping region.

Acknowledgment

The authors (Shahid M Ramay and Asif Mahmood) extend their appreciation to the Deanship of Scientific Research at King Saud University for funding the work through the research group project No. RG-1435-004.

References

[1] Jungwirth T, Sinova J, Mašek J, Kušra J and MacDonald A H 2006 *Rev. Mod. Phys.* **78** 809
[2] Celik O, Tiras E, Ardali S, Lisesivdin S B and Ozbay E 2011 *Phys. Status Solidi C* **8** 1625
[3] Saini H S, Singh M, Reshak A H and Ashyap M K 2012 *J. Alloys. Compnd.* **536** 214
[4] Fan S W, Yao K L, Huang Z G, Zhang J, Gao G Y and Du G H 2009 *Chem. Phys. Lett.* **482** 62

[5] Kulatov E, Nakayama H, Mariette H, Ohta H and Uspenskii Y A 2002 *Phys. Rev. B* **66** 045203
[6] Ronning C, GaoP X, Ding Y, Wang Z L and Schwen D 2004 *Appl. Phys. Lett.* **84** 783
[7] Esmaeili M, Gholam M, Haratizadeh H, *et al*. 2009 *Opto-Electron. Rev.* **17** 293
[8] Jiang H X and Lin J Y 2002 *Opto-Electron. Rev.* **10** 271
[9] Wu J, Haller E E, Lu H, Schaff W J, Saito Y and Nanishi Y 2002 *Appl. Phys. Lett.* **80** 3967
[10] Matsuoka T, Okamoto H, Nakao M, Harima H and Kurimoto E 2002 *Appl. Phys. Lett.* **81** 1246
[11] Amin B, Ahmad I, Maqbool M, Goumri-Said S and Ahmad R 2011 *J. Appl. Phys.* **109** 023109
[12] Kanaya H, Yaguchi H, Hijikata Y, Yoshida S, Miyoshi S and Onabe K 2003 *Phys. Status Solidi (c)* **7** 2753
[13] Shan W, Walukiewicz W, Yu K M, Wu J, Ager J W III, Haller E E, Xin H P and Tu C W 2000 *Appl. Phys. Lett.* **76** 3251
[14] Kent P R C and Zunger A 2001 *Phys. Rev. B* **64** 115208
[15] Rudko Yu G, Buyanova I A, Chen W M, Xin H P and Tu C W 2002 *Appl. Phys. Lett.* **81** 3984
[16] Yoon S, Seong M J, Geisz J F, Duda A and Mascarenhas A 2003 *Phys. Rev. B* **67** 235209
[17] Leibiger G, Gottschalch V, Schubert M, Benndorf G and Schwabe R 2002 *Phys. Rev. B* **65** 245207
[18] Adachi S 2005 *Properties of group-IV, III–V and II–VI semiconductors, series in materials for electronic and optoelectronic application*, MS Dissertation (New York)
[19] Madelung O 1996 *Semiconductors–Basic Data*, 2nd edn. (Berlin: Springer)
[20] Lyons J L, Janotti A and Van de Walle C G 2014 *Phys. Rev. B* **89** 035204
[21] Moon R L, Antypasj G A and James L W 1974 *J. Electron. Mater.* **3** 635
[22] Laref A, Hussain Z, Laref S, Yang J T, Xiong Y C and Luo S J 2018 *J. Phys. Chem. Solids* **115** 352
[23] Omkar J, Ian F, Christiana H and Sarah K 2007 *Appl. Phys. Lett.* **91** 132117
[24] Murayama M and Nakayama T 1994 *Phys. Rev. B* **49** 4710
[25] Sibirev N V, Timofeeva W A, Bolshakov A D, Nazarenko M V and Dubrovskii V 2010 *Phys. Solid. State* **52** 1531
[26] De Vos A 1992 *Endoreversible Thermodynamics of Solar Energy Conversion* (Oxford: Oxford University Press)
[27] Laref A, Altujar A, Laref S and Luo S J 2017 *Solar Energy* **142** 231
[28] Laref A, Altujar A and Luo S J 2014 *Appl. Phys. A* **117** 1451
[29] Ernzerhof M and Scuseria E G 1999 *J. Chem. Phys.* **110** 5029
[30] Tran F and Blaha P 2009 *Phys. Rev. Lett.* **102** 226401
[31] Kohn W and Sham L 1965 *J. Phys. Rev.* **140** 1133
[32] Perdew J P and Burke K M 1996 *Phys. Rev. Lett.* **77** 3865
[33] Becke A D 1993 *J. Chem. Phys.* **98** 1372
[34] Ropo M, Kokko K and Vitos L 2008 *Phys. Rev. B* **77** 195445
[35] Anisimov V I, Zaanen J and Andersen O K 1991 *Phys. Rev. B* **44** 943
[36] Tran F and Blaha P 2009 *Phys. Rev. Lett.* **102** 226401
[37] Koller D, Tran F and Blaha P 2012 *Phys. Rev. B* **85** 155109
[38] Tian F, Lin D Y, Gao X, Zhao Y F and Song H F 2020 *J. Chem. Phys.* **153** 034101
[39] Vitiello S A, Runge K J, Chester G V and Kalos M H 1990 *Phys. Rev. B* **42** 228
[40] Laref A, Altujar A and Luo S J 2014 *Appl. Phys. A* **117** 1451
[41] Al-Douri Y 2013 *Procedia Engineering* **53** 400
[42] Ziane M I, Bensaad Z, Labdelli B and Bennacer H 2014 *Sensors Transducers* **27** 374
[43] Said A, Debbichi M and Said M 2016 *Optik* **127** 9212
[44] Yangyz Z and Xu Z 1996 *J. Phys.: Condens. Matter* **8** 8303
[45] Gorczyca I, Suski T, Strak P, Staszczak G and Christensen N E 2017 *Sci. Rep.* **7** 16055
[46] Magnuson M, Mattesini M, Hoglund C, Birch J and Hultman L 2010 *Phys. Rev. B* **81** 085125
[47] Rinke P, Scheffler M, Qteish A, Winkelnkemper M, Bimberg D and Neugebauer J 2006 *Appl. Phys. Lett.* **89** 161919
[48] Inushima T, Mamutin V V, Vekshin V A, Ivanov S V, Sakon T, Motokawac M and Ohoya S 2001 *J. Crystal Growth* **227–228** 481
[49] Mahmood Q, Rashid M, Hassan M, Yaseen M, Laref A and Haq B U 2019 *Phys. Scr.* **94** 105812
[50] Kaf A, Khodja F D, Saadaoui F, Chibani S, Bentayeb A and Khodja M D 2020 *J. Comput. Electron.* **19** 26
[51] Haq B U, Ahmed R, Shaari A, Hassan F E H, Kanounc M B and Goumri-Said S 2014 *Solar Energy* **107** 543
[52] Reshak H A, Mikhail Y S, Saeed Y, Kityk I V and Auluck S 2011 *J. Phys. Chem. B* **115** 2836
[53] Wooten F 1972 *Optical Properties of Solids* (New York: Academic)
[54] Penn D R 1962 *Phys. Rev.* **128** 2093
[55] Cai M M, Yin Z and Zhang M S 2003 *Appl. Phys. Lett.* **83** 2805
[56] Bhamu K C, Soni A and Sahariya J 2018 *Solar Energy* **162** 336
[57] Haq B U, Ahmed R and Goumri-Said S 2014 *Solar Energy Mater. Solar Cells* **130** 6
[58] Ali N, Ahmed R, Haq B U, Shaari A, Hussain R and Goumri-Said S 2015 *Solar Energy* **113** 25
[59] Rehman S U, Butt F K, Haq B U, AlFaify S, Khan W S and Li C 2018 *Solar Energy* **169** 648
[60] Haq B U, Ahmed R, Hassan F El H, Khenata R, Kasmin M K and Goumri-Said S 2014 *Solar Energy* **100** 1
[61] Yao H, Snyder P G and Woollam J A 1991 *J. Appl. Phys.* **70** 3261
[62] Mahmood Q, Rouf S A, Rashid M, Sajjad M, Jamil M and Laref A 2019 *Zeitschrift fur Naturforschung* September 2, 2019